

Contrastive-Based Deep Embeddings for Label Noise-Resilient Histopathology Image Classification

Lucas Dedieu¹

Nicolas Nerrienet¹

Adrien Nivaggioli¹

Clara Simmat¹

Marceau Clavel¹

Arnaud Gauthier^{1,2}

Stéphane Sockeel¹

Rémy Peyret¹

¹ *Prima, Paris, France*

² *Diagnostic and Theranostic Medicine Division, Department of Pathology, Institut Curie, PSL University, Paris, France*

LUCAS@PRIMAALAB.COM

NICOLAS.N@PRIMAALAB.COM

ADRIEN@PRIMAALAB.COM

CLARA@PRIMAALAB.COM

MARCEAU@PRIMAALAB.COM

ARNAUD@PRIMAALAB.COM

STEPHANE@PRIMAALAB.COM

REMY@PRIMAALAB.COM

Abstract

Recent advancements in deep learning have proven highly effective in medical image classification, notably within histopathology. However, noisy labels represent a critical challenge in histopathology image classification, where accurate annotations are vital for training robust deep learning models. Indeed, deep neural networks can easily overfit label noise, leading to severe degradations in model performance. While numerous public pathology foundation models have emerged recently, none have evaluated their resilience to label noise. Through thorough empirical analyses across multiple datasets, we exhibit the label noise resilience property of embeddings extracted from foundation models trained in a self-supervised contrastive manner. We demonstrate that training with such embeddings substantially enhances label noise robustness when compared to non-contrastive-based ones as well as commonly used noise-resilient methods. Our results unequivocally underline the superiority of contrastive learning in effectively mitigating the label noise challenge. Code is publicly available at <https://github.com/LucasDedieu/NoiseResilientHistopathology>

Keywords: Histopathology, Image Classification, Label Noise, Contrastive Learning, Deep Embeddings, Foundation Models

1. Introduction

Histopathology, the microscopic examination of tissue samples, plays a crucial role in the diagnosis, prognosis, and treatment of various diseases, including cancer. With the rise of digital pathology thanks to whole-slide image (WSI) scanners, image analysis and deep learning are becoming part of histopathologists' routine. As the workload of histopathologists has grown significantly in previous decades (Garcia et al., 2020), deep learning-based image analysis now plays a major role in increasing clinical workflow efficiency (Dawson, 2022). To be effective, training such deep neural networks (DNNs) requires large image datasets with reliable labels. However, in the context of medical imaging and histopathology in particular, clean data are rare and expensive, requiring expert labeling campaigns.

Thus, one of the key challenges in histopathology image analysis is the presence of label noise, which refers to errors or inaccuracies in the annotations provided for the training data. These inaccuracies, stemming from inter-observer variability, imperfect segmentation of tissue regions, inherent ambiguity in the biological features, and omission errors, impede the development of reliable deep learning models. Indeed, it has been proven that DNNs can easily overfit noisy labels (Li et al., 2018; Zhang et al., 2016), leading to severe degradations in model performance and thus potentially misleading clinical decisions.

To mitigate this challenge, various approaches have been proposed in the literature, ranging from robust loss functions to novel training methodologies and label cleaning strategies. In more recent works, self-supervised-based methods also emerged. Nevertheless, the quest for noise-tolerant models in the presence of label noise remains an ongoing pursuit.

In this paper, we aim to comprehensively evaluate the robustness of deep embeddings extracted from pretrained backbones specifically designed for histopathology image classification. We compare the noise tolerance of models trained solely on these features to those trained on the original images and assess their performance on multiple histopathology datasets. Our key contributions are: (1) We demonstrate that classifiers trained on contrastive deep embeddings exhibit improved robustness to label noise compared to those trained on the original images using state-of-the-art methods. This highlights the inherent noise resilience of these features. (2) We compare the noise robustness of contrastive embeddings to alternative self-supervised embeddings extracted from non-contrastive backbones, demonstrating the superior ability of contrastive-based backbones to handle noisy labels.

2. Related Work

2.1. Learning with Noisy Labels Methods

In image classification, a multitude of approaches have been explored to enhance the robustness of learning algorithms in the presence of noisy labels.

Label Cleaning Strategies: CleanNet (Lee et al., 2017) uses a small, clean dataset to generate feature vectors for each class, comparing them with query image vectors to determine label accuracy. Rank Pruning (Northcutt et al., 2017) focuses on high-confidence data points for classifier training, potentially overlooking challenging samples common in medical tasks. To overcome this, Zhu et al. (2022) propose a two-phase hard sample aware noise robust learning algorithm consisting in an easy/hard/noisy detection scheme combined with a noise suppressing and hard enhancing scheme.

Robust Loss Functions: Other methods focus on changing the loss function, such as Ghosh et al. (2017) that showed that the categorical cross entropy (CCE) loss is sensitive to label noise while the mean absolute error (MAE) loss is robust. However, training a network under MAE loss leads to underfitting and thus Zhang and Sabuncu (2018) proposed generalized cross entropy (GCE), a noise-robust loss function that can be seen as a generalization of MAE and CCE. In the same way, Ma et al. (2020) showed that every loss can be noise-robust through simple normalization, but may lead to an underfitting problem. To tackle this challenge, the authors introduce a synergistic boosting framework that enables the development of a novel family of loss functions, each possessing the theoretical guarantee of robustness while maintaining efficient learning.

Training Procedures: Numerous studies also explored novel training approaches to address the issue of label noise. Co-teaching (Han et al., 2018) proposed a new deep learning paradigm that involves maintaining two neural networks in parallel and selecting instances with low loss values for cross-training. Improving this work, Co-teaching+ (Yu et al., 2019) bridges "update by disagreement" strategy with the original Co-teaching. Also using two networks, DivideMix (Li et al., 2020) employs a mixture model to dynamically partition the training data into clean and noisy subsets, enabling semi-supervised learning on both. To address confirmation bias, the two networks are trained separately, each using the other network’s dataset division.

2.2. Self-Supervised-Based Methods

Some recent works leverage advances in self-supervised learning (SSL) to deal with noisy labels. SSL is a paradigm in which models are trained from unlabeled data using pretext tasks. By solving these pretext tasks, models learn meaningful representations of the data and the acquired knowledge is then transferred to the primary task of classification or segmentation. Tackling label noise, Co-learning (Tan et al., 2021) trains two classifier heads with a shared feature encoder and regularizes the model with both the intrinsic similarity and the structural similarity. Kurian et al. (2022) use a contrastive learning framework and feature aggregating memory banks to identify and increase the emphasis on clean training samples. Jiang et al. (2023) integrate contrastive learning and intra-group attention mixup techniques into standard supervised learning. Khanal et al. (2023) showed that model pretraining with SimCLR (Chen et al., 2020a) consistently yields the best results in presence of noisy labels on two medical datasets.

The reasons behind the enhancement of label noise resilience through contrastive learning are still not fully understood, and as far as our knowledge extends, only one study (Xue et al., 2022) has delved into the theoretical understanding of this achievement. The authors demonstrated that contrastive learning yields a representation matrix characterized by a significant gap between the prominent singular values and the remaining ones, along with a considerable alignment between the prominent singular vectors and the accurate labels. Aforementioned characteristics enable a linear classifier head trained on these representations to adeptly learn clean labels while minimizing overfitting to the noisy ones.

2.3. Pathology Foundation Models

The emergence of SSL has been particularly impactful in the domain of histology, where obtaining large amounts of accurately labeled data is challenging and expensive. In the last few years, many foundation models trained in a self-supervised way have been developed. Wang et al. (2022, 2021) introduced CTransPath, a feature extractor based on the swin transformer (Liu et al., 2021), trained on TCGA (Weinstein et al., 2013) and PAIP (Kim et al., 2021) using semantically-relevant contrastive learning (SRCL), a novel SSL technique adapted from MoCo v3 (Chen et al., 2021) specifically designed for pathology applications. They also presented RetCCL (Wang et al., 2023), a ResNet-50 (He et al., 2015) model trained on the same two datasets using their clustering-guided contrastive learning (CCL) SSL technique, which was based on MoCo (He et al., 2020). Filot et al. (2023) evaluated various vision transformer (ViT) variants (Kolesnikov et al., 2021) on TCGA using the iBOT

framework (Zhou et al., 2022) and mask image modeling, a new paradigm of SSL coming from the world of natural language processing (NLP) applied to vision. Authors named their most effective ViT-B variant "Phikon". Lunit (Kang et al., 2023) conducted a benchmark of several SSL techniques, including Barlow Twins (Zbontar et al., 2021), SwAV (Caron et al., 2020), MoCo v2 (Chen et al., 2020b), and DINO (Caron et al., 2021) (self-distillation), for pathology by training them on TCGA. Hua et al. (2023) trained Pathoduet on TCGA using newly-introduced pretext tokens and later task raisers to explicitly utilize certain relations between images and showed better results than CTransPath on some patch classification tasks. In recent months, several other pathology foundation models have emerged, trained on much larger datasets (Chen et al., 2023; Vorontsov et al., 2023; Dippel and Feulner, 2024; Campanella and Kwan, 2023; Lu et al., 2023). Regrettably, we could not incorporate these models into our research due to their proprietary nature.

3. Proposed Approach

3.1. Problem Formulation

Given a K -class image classification problem, let $\mathcal{X} \subset \mathbb{R}^d$ be the image space, and let $\mathcal{Y} = \{1, \dots, K\}$ be the class labels. In a typical learning scheme, we are given training data, $S = \{(\mathbf{x}, y)^{(i)}\}_{i=1}^N \in (\mathcal{X} \times \mathcal{Y})^N$. Classification aims to learn a function $f : \mathcal{X} \rightarrow \mathcal{Y}$ (represented by a DNN) that maps the input space to the label space. Training model f involves finding optimal parameters θ minimizing the empirical risk, i.e., $\theta := \arg \min_{\theta} \sum_{i=1}^N \mathcal{L}(f(\mathbf{x}_i), y_i)$, where $\mathcal{L}(f(\mathbf{x}), y)$ is the loss of f with respect to y .

In presence of uniform label noise, the noisy training data available to the classifier is $S_{\eta} = \{(\mathbf{x}, \hat{y})^{(i)}\}_{i=1}^N$, where $\eta \in [0, 1]$ denotes the uniform noise rate in the dataset, and

$$\hat{y}_i = \begin{cases} y_i & \text{with probability } (1 - \eta) \\ k, k \neq y_i & \text{with probability } p_{\eta} = \frac{\eta}{K-1} \end{cases} \quad (1)$$

Remark 1 We do not consider a uniform noise rate $\eta > \frac{K-1}{K}$ as, for balanced dataset, it would mean that for each class k , $\exists c \neq k$, where c has more data labeled as class k than k .

In asymmetric label noise scenarios, the flipping probabilities of each class are conditioned by a transition matrix T , thus $p_{\eta} = T_{y_i, k}$ represents the probability of transitioning from true label y_i to noisy label k . Asymmetric label noise tends to provide a more realistic representation of real-world noise scenarios as certain classes may be more prone to confusion due to visual similarity or contextual ambiguity.

3.2. Learning with Contrastive-Based Deep Embeddings

To mitigate label noise, we propose an approach based on contrastive-based deep embeddings. We employ a contrastive-pretrained backbone to extract embeddings from images and then exploit these embeddings and corresponding noisy labels to train a linear classifier head. Here, $f = h \circ g$ with $g : \mathcal{X} \rightarrow \mathcal{B}$, the frozen backbone parameterized by θ_g and $h : \mathcal{B} \rightarrow \mathcal{Y}$, the classifier head parameterized by θ_h . \mathcal{B} represents the latent space of embeddings. The main advantage of this training approach is that it allows to use the same

pre-trained feature extractor g for multiple datasets, and only train a separate classifier h_i for each dataset $i = 1, \dots, M$. It enables significantly faster trainings since the latent space \mathcal{B} and parameters θ_h are much smaller than the image space \mathcal{X} and θ .

4. Experiments

In this section, we propose a comparison of different methods for handling noisy labels. We benchmark four image-based methods: a baseline, GCE, Active-Passive loss (APL), and DivideMix. In addition, we compare eight deep embedding methods based on eight foundation models. These include four contrastive histology backbones: RetCCL, CTransPath, PathoDuet, and Lunit Barlow Twins (BT); two non-contrastive histology backbones: Phikon and Lunit DINO; and two ViT-B models trained on ImageNet (Deng et al., 2009) with MoCo v3 (contrastive) and iBOT (non-contrastive). We include the two ImageNet models to also investigate the performance of contrastive and non-contrastive embeddings derived from backbones in unrelated domains. The experimental settings are detailed in appendix A.

4.1. Datasets and Pre-processing

We validate the effectiveness of our proposed approach by assessing its performance on six public benchmark datasets, namely NCT-CRC-HE-100K (Kather et al., 2018), PatchCamelyon (Veeling et al., 2018), BACH (Polónia et al., 2020), MHIST (Wei et al., 2021), LC25000 (Borkowski et al., 2019) and GasHisSDB (Hu et al., 2022). Table 1, summarizes all dataset details. We add more information about these datasets and the pre-processing used in appendix B.

Table 1: Dataset details. [†] set obtained from train set split, [‡] set labelled by a pathologist expert for this study.

Dataset	Patch Size	Train	Validation	Test	K
NCT-CRC-HE-100k	224x224	80,000	20,000 [†]	7,180	9
PatchCamelyon	96x96	262,144	32,768	32,768	2
BACH	2048x1536	320	80 [†]	83 [‡]	4
MHIST	224x224	1740	435 [†]	977	2
LC25000	768x768	16,000	4000 [†]	5000 [†]	5
GasHisSDB	160x160	21,303	5325 [†]	6656 [†]	2

4.2. Results

The results under uniform label noise, as depicted in Table 2, highlight the efficacy of training with deep embeddings. Across nearly all the datasets and noise rates scenarios, these methods consistently match or surpass performances of image-based approaches. Particularly noteworthy is the observation that, for noise rates $\eta > 0$, classifiers trained with contrastive embeddings exhibit superior performance compared to their non-contrastive counterparts. This phenomenon is graphically illustrated in Figure 1, providing a finer-grained insight into the impact of noise rates. Across all datasets, the accuracies of Phikon and Lunit-DINO (non-contrastive) consistently exhibit sharper declines compared to others.

Table 2: Average test accuracies with standard deviation under different uniform label noise ratios (% , 2 runs for image methods, 4 runs for deep embedding methods). *Foundation model trained with contrastive learning.

Method	NCT-CRC-HE-100k					PatchCamelyon		
	$\eta = 0$	$\eta = 0.2$	$\eta = 0.4$	$\eta = 0.6$	$\eta = 0.8$	$\eta = 0$	$\eta = 0.2$	$\eta = 0.4$
Baseline	96.7 \pm 0.1	90.4 \pm 0.7	83.2 \pm 1.7	70.9 \pm 6.1	35.5 \pm 0.3	87.3 \pm 2.1	85.9 \pm 1.0	73.1 \pm 1.8
GCE	96.8 \pm 0.2	96.1 \pm 0.5	94.8 \pm 0.4	93.4 \pm 0.2	82.9 \pm 5.3	85.5 \pm 1.1	85.2 \pm 1.6	82.8 \pm 1.0
APL	96.4 \pm 0.1	96.6 \pm 0.1	96.2 \pm 0.1	95.1 \pm 0.2	8.8 \pm 0.1	89.1 \pm 0.1	86.4 \pm 0.4	81.2 \pm 3.3
DivideMix	97.1 \pm 0.1	96.9 \pm 0.1	96.4 \pm 0.2	96.3 \pm 0.2	94.7 \pm 1.7	90.3 \pm 0.1	87.4 \pm 0.2	87.0 \pm 0.7
Phikon	94.3 \pm 0.6	92.2 \pm 1.4	88.4 \pm 5.2	82.6 \pm 4.0	40.9 \pm 11.2	86.4 \pm 0.7	82.5 \pm 1.3	77.6 \pm 2.2
RetCCL*	94.5 \pm 0.1	95.1 \pm 0.2	95.2 \pm 0.1	94.8 \pm 0.2	93.6 \pm 0.3	85.8 \pm 0.7	84.5 \pm 0.2	82.7 \pm 0.6
Lunit-DINO	95.4 \pm 0.5	95.0 \pm 0.6	93.3 \pm 3.1	86.6 \pm 8.3	61.6 \pm 8.8	88.1 \pm 1.4	85.5 \pm 0.3	80.1 \pm 2.6
Lunit-BT*	94.3 \pm 0.3	94.7 \pm 0.3	94.4 \pm 0.3	94.1 \pm 0.4	92.3 \pm 0.8	91.0\pm0.2	90.7\pm0.2	89.2\pm0.1
CTransPath*	97.4\pm0.2	97.4\pm0.2	97.4\pm0.2	96.9\pm0.1	95.1\pm0.3	89.0 \pm 0.5	87.0 \pm 0.8	85.2 \pm 1.5
PathoDuet*	96.1 \pm 0.4	96.3 \pm 0.2	95.9 \pm 0.3	95.5 \pm 0.2	93.3 \pm 0.8	87.1 \pm 0.5	87.0 \pm 0.2	85.8 \pm 0.4
iBOT	93.3 \pm 0.5	90.1 \pm 1.2	84.6 \pm 4.4	78.3 \pm 6.2	45.1 \pm 10.2	83.2 \pm 0.5	77.8 \pm 1.9	68.9 \pm 1.9
MoCo*	93.2 \pm 0.5	93.0 \pm 1.1	90.8 \pm 1.4	88.8 \pm 0.4	86.0 \pm 0.4	81.2 \pm 0.3	80.1 \pm 0.4	78.6 \pm 0.5

Method	BACH				MHIST		
	$\eta = 0$	$\eta = 0.2$	$\eta = 0.4$	$\eta = 0.6$	$\eta = 0$	$\eta = 0.2$	$\eta = 0.4$
Baseline	78.2 \pm 2.1	65.1 \pm 3.4	41.3 \pm 6.9	40.5 \pm 6.3	82.9 \pm 0.9	72.1 \pm 3.1	60.2 \pm 0.7
GCE	76.9 \pm 0.2	68.5 \pm 1.8	61.3 \pm 1.5	52.3 \pm 2.7	84.3 \pm 0.6	76.9 \pm 0.6	59.2 \pm 6.7
APL	77.5 \pm 0.6	73.1 \pm 0.6	64.6 \pm 2.3	51.7 \pm 4.9	83.8 \pm 0.9	72.1 \pm 8.9	68.2 \pm 0.6
DivideMix	79.6 \pm 0.1	73.8 \pm 2.0	64.9 \pm 3.1	50.9 \pm 2.1	84.2 \pm 0.2	80.9\pm0.4	72.2 \pm 1.4
Phikon	77.4 \pm 1.3	69.3 \pm 2.2	55.1 \pm 9.7	40.0 \pm 4.8	84.5\pm0.5	75.0 \pm 0.9	57.9 \pm 4.8
RetCCL*	73.5 \pm 0.5	71.7 \pm 0.3	68.7 \pm 1.7	61.0 \pm 1.3	81.2 \pm 0.7	78.1 \pm 1.2	73.0 \pm 3.5
Lunit-Dino	80.7 \pm 0.1	72.8 \pm 2.1	58.7 \pm 3.6	41.0 \pm 3.5	79.1 \pm 2.1	75.1 \pm 1.8	64.3 \pm 4.1
Lunit-BT*	81.2 \pm 1.3	78.7 \pm 0.9	74.3 \pm 1.5	65.7 \pm 1.9	79.6 \pm 0.4	78.1 \pm 1.5	76.0\pm0.8
CTransPath*	83.7\pm0.6	80.4\pm1.6	77.2\pm1.3	72.3\pm1.0	80.4 \pm 0.6	79.6 \pm 0.7	75.1 \pm 1.2
PathoDuet*	79.0 \pm 2.5	75.4 \pm 2.1	72.7 \pm 2.2	68.0 \pm 1.8	78.3 \pm 1.0	76.4 \pm 0.9	71.1 \pm 3.5
iBOT	79.2 \pm 2.0	62.7 \pm 5.2	51.2 \pm 4.7	34.0 \pm 7.7	82.1 \pm 0.7	72.3 \pm 1.9	56.8 \pm 1.2
MoCo*	71.2 \pm 0.5	68.8 \pm 1.2	65.6 \pm 1.4	58.2 \pm 1.5	78.2 \pm 0.5	76.1 \pm 1.2	72.6 \pm 1.4

Method	LC25000				GasHisSDB		
	$\eta = 0$	$\eta = 0.2$	$\eta = 0.4$	$\eta = 0.6$	$\eta = 0$	$\eta = 0.2$	$\eta = 0.4$
Baseline	100\pm0.0	95.0 \pm 0.4	77.5 \pm 3.7	75.8 \pm 4.2	98.2 \pm 0.4	87.7 \pm 0.2	65.5 \pm 2.4
GCE	99.9 \pm 0.1	99.8\pm0.1	99.4 \pm 0.2	96.9 \pm 0.2	98.3 \pm 0.1	96.0 \pm 0.2	74.9 \pm 5.0
APL	99.9 \pm 0.1	99.7 \pm 0.1	99.4 \pm 0.1	98.1 \pm 0.2	98.1 \pm 0.1	96.5 \pm 0.1	75.4 \pm 0.5
DivideMix	99.7 \pm 0.2	99.6 \pm 0.1	99.4 \pm 0.2	98.4 \pm 0.1	97.9 \pm 0.1	97.3\pm0.1	93.5 \pm 0.4
Phikon	99.9 \pm 0.1	99.6 \pm 0.1	99.1 \pm 0.1	97.7 \pm 0.5	99.6\pm0.1	86.7 \pm 1.5	64.9 \pm 1.6
RetCCL*	98.7 \pm 0.2	97.8 \pm 0.2	97.6 \pm 0.2	97.0 \pm 0.2	97.2 \pm 0.1	95.3 \pm 0.5	87.3 \pm 2.5
Lunit-DINO	99.6 \pm 0.2	99.1 \pm 0.1	99.0 \pm 0.1	97.2 \pm 0.6	99.2 \pm 0.1	84.9 \pm 2.1	65.7 \pm 2.2
Lunit-BT*	99.9 \pm 0.1	99.6 \pm 0.3	99.1 \pm 0.1	98.6 \pm 0.1	98.5 \pm 0.1	97.2 \pm 0.3	91.6 \pm 3.2
CTransPath*	99.9 \pm 0.1	99.3 \pm 0.2	99.1 \pm 0.1	98.9\pm0.1	98.7 \pm 0.1	97.3\pm0.2	94.6\pm0.3
PathoDuet*	99.9 \pm 0.1	99.8\pm0.1	99.6\pm0.1	98.5 \pm 0.1	98.3 \pm 0.1	95.9 \pm 0.9	92.4 \pm 1.1
iBOT	99.9 \pm 0.1	95.7 \pm 1.3	89.2 \pm 0.7	67.8 \pm 8.2	97.3 \pm 0.4	80.1 \pm 1.2	60.6 \pm 3.8
MoCo*	98.5 \pm 0.1	98.2 \pm 0.1	97.9 \pm 0.1	97.4 \pm 0.2	96.2 \pm 0.2	91.0 \pm 0.4	85.9 \pm 0.6

One might think that these two models extract inferior representations compared to others. However, we demonstrate that this is not true through a few-shot learning experiment using k-nearest neighbors (k-NN) classifiers trained on 10% of each dataset. Idea is to test the inherent resistance of embeddings and demonstrate that, without proper training of a

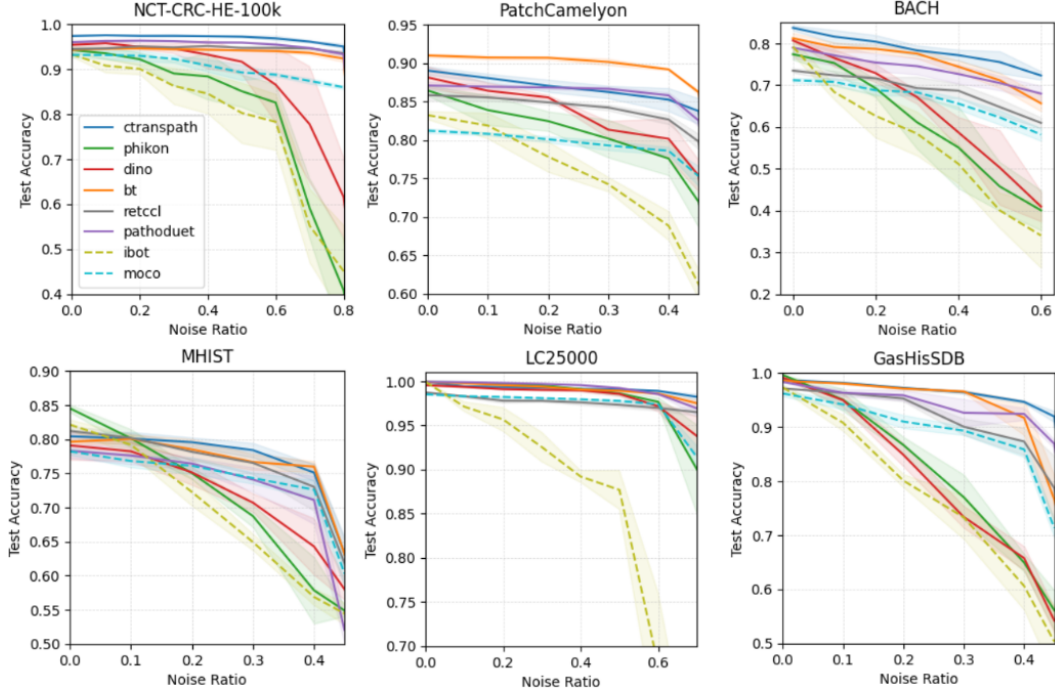


Figure 1: Average test accuracies (4 runs) of linear classifiers trained with deep embedding over different label noise ratios. Shaded areas represent standard deviation. iBOT and MoCo backbones (dashed curves) are pre-trained on ImageNet.

linear head, they exhibit uniform reactions to label noise. Results, illustrated in Figure 2, confirm that hypothesis. Furthermore, upon closer examination through t-SNE visualization of NCT-CRC-HE-100k in Figure 3 it becomes evident that no model extracts a worse representation. Thus the observed performance differences are not due to the quality of the learned representations, but rather to the noise-resilient property leveraged by the linear classifier when trained with contrastive embeddings.

That explains why in Figure 1, at $\eta = 0$, Phikon and Lunit-DINO perform really well but, at higher noise rates, some contrastive methods start with lower accuracies than them at $\eta = 0$, yet subsequently outpace them, thereby showcasing their enhanced resilience to label noise. A particularly prominent example is PatchCamelyon with RetCCL, where the test accuracy starts at 85.8%, while Phikon and Lunit-DINO start at 86.4% and 88.1%. However, RetCCL maintains stability as η increases, while the other two decline. Under asymmetric noise, the conclusion is consistent with the previous observations as shown in Table 3. Specifically, on the three multiclass datasets, training with contrastive deep embeddings yields the best results. Moreover, the results on the two ImageNet backbones under both noise types further support our findings, with iBOT exhibiting a consistently steeper decline in performance than MoCo as the noise rate increases.

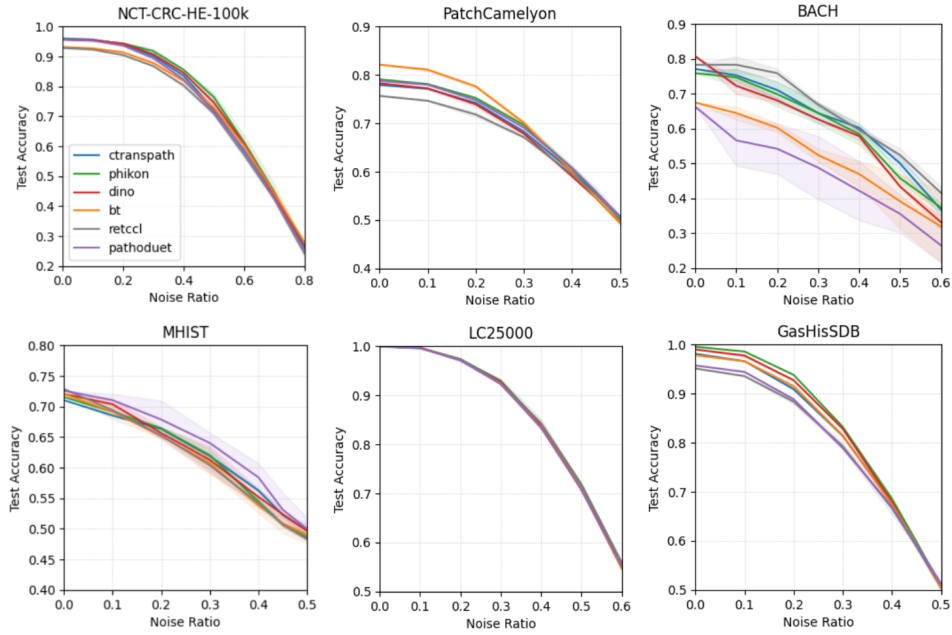


Figure 2: Average test accuracies (4 runs) of k-NN classifiers ($k=5$) trained on 10% of train datasets over different label noise ratios. Shaded areas represent standard deviation.

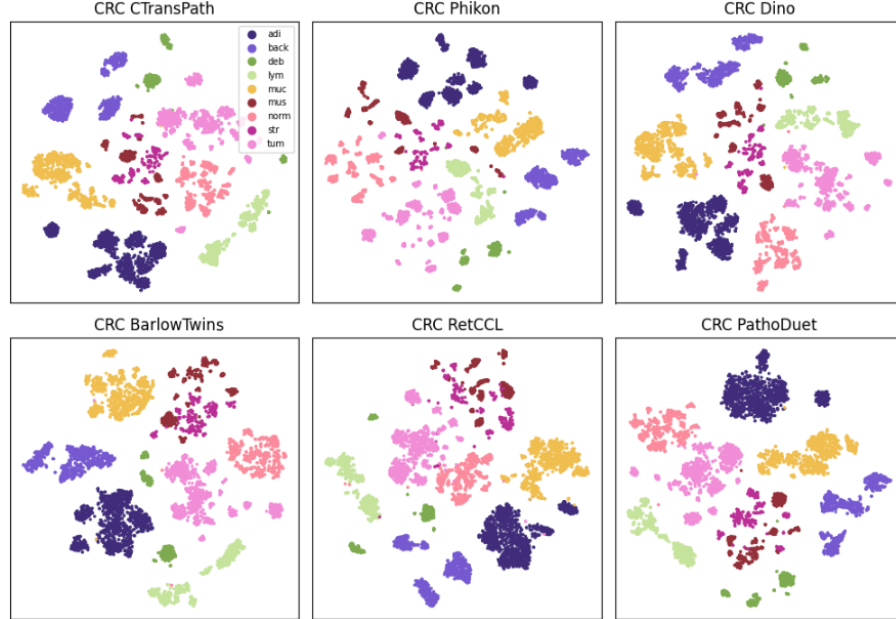


Figure 3: t-SNE representations of NCT-CRC-HE-100k deep embeddings extracted from various histopathology foundation models.

Table 3: Average test accuracies with standard deviation on NCT-CRC-HE-100k, BACH and LC25000 under different asymmetric label noise ratios (% , 2 runs for image methods, 4 runs for deep embedding methods). Class transition matrices are given in appendix C.
 *Foundation model trained with contrastive learning.

Method	NCT-CRC-HE-100k		BACH		LC25000	
	$\eta = 0.2$	$\eta = 0.4$	$\eta = 0.2$	$\eta = 0.4$	$\eta = 0.2$	$\eta = 0.4$
Baseline	88.6 \pm 0.9	78.4 \pm 1.3	60.4 \pm 4.1	40.2 \pm 8.4	95.1 \pm 1.1	69.3 \pm 1.2
GCE	94.5 \pm 0.3	91.3 \pm 1.7	65.4 \pm 1.3	56.8 \pm 2.7	97.2 \pm 0.1	92.7 \pm 0.4
APL	94.5 \pm 0.4	92.0 \pm 0.3	70.5 \pm 0.9	60.7 \pm 2.2	97.2 \pm 0.3	93.4 \pm 0.5
DivideMix	96.0 \pm 0.1	95.4 \pm 0.2	72.4 \pm 1.5	61.3 \pm 2.0	98.9 \pm 0.1	96.5 \pm 0.2
Phikon	88.0 \pm 4.1	74.9 \pm 7.8	66.9 \pm 3.5	46.7 \pm 3.6	98.9 \pm 0.1	96.3 \pm 0.7
RetCCL*	93.9 \pm 0.4	93.4 \pm 0.3	77.4 \pm 1.6	61.4 \pm 5.2	97.6 \pm 0.1	96.8 \pm 0.2
Lunit-DINO	93.1 \pm 2.6	85.7 \pm 6.4	65.1 \pm 4.1	51.2 \pm 3.9	99.1 \pm 0.1	97.3 \pm 0.2
Lunit-BT*	94.5 \pm 0.2	94.2 \pm 0.7	69.3 \pm 4.0	57.5 \pm 8.4	99.5 \pm 0.1	97.9 \pm 0.3
CTransPath*	97.4\pm0.2	97.1\pm0.3	79.0\pm1.3	66.9\pm14.7	99.2 \pm 0.3	98.5\pm0.1
PathoDuet*	95.8 \pm 0.3	95.6 \pm 0.4	73.1 \pm 0.8	62.2 \pm 3.5	99.6\pm0.1	98.1 \pm 0.7
iBOT	82.4 \pm 3.4	66.9 \pm 8.7	58.6 \pm 4.6	45.8 \pm 3.5	93.1 \pm 3.3	77.5 \pm 3.1
MoCo*	92.9 \pm 0.3	91.2 \pm 0.4	66.8 \pm 0.6	62.3 \pm 1.4	92.5 \pm 4.2	88.3 \pm 2.4

5. Limitations

Although the study shows that contrastive learning effectively mitigates the label noise challenge, it does not completely eliminate it. Specifically, for relatively small datasets such as BACH and MHIST, the stability over varying noise rates is lower than the one observed with larger datasets. Similarly, asymmetric noise appears to be more challenging to resist. Thus, there is still a need for further research to develop methods that can completely overcome the label noise issue. Potential avenues for future research include exploring the combination of contrastive embeddings with other noise resilience methods such as label cleaning or robust losses or investigating the impact of fine-tuning the non-contrastive backbones with contrastive learning. For control over noise rates we used synthetic label noise over public datasets. A validation study using real-world noisy datasets could conclude into the effectiveness of contrastive embeddings in handling label noise.

6. Conclusion

Our study highlights the effectiveness of contrastive-based deep embedding training in bolstering the robustness of histopathology classifiers under noisy labels. Through extensive experiments across multiple benchmark datasets, we showcase the superior noise resilience of linear classifiers trained with contrastive-based deep embeddings when compared to image-based methods and non-contrastive embeddings. By elucidating these findings, our aim is to offer valuable insights and guidelines for the future development of histopathological foundation models. Notably, the majority of current histology foundation models overlook the assessment of label noise resilience in their performance evaluations, despite it being one of the most significant challenges in digital histopathology.

Acknowledgments

This work was supported by Primaa.

References

- Andrew A. Borkowski, Marilyn M. Bui, L. Brannon Thomas, Catherine P. Wilson, Lauren A. DeLand, and Stephen M. Mastorides. Lung and colon cancer histopathological image dataset (lc25000), 2019.
- Gabriele Campanella and Ricky Kwan. Computational pathology at health system scale – self-supervised foundation models from three billion images, 9 2023.
- Mathilde Caron, Ishan Misra, Julien Mairal, Priya Goyal, Piotr Bojanowski, and Armand Joulin. Unsupervised learning of visual features by contrasting cluster assignments. 2020.
- Mathilde Caron, Hugo Touvron, Ishan Misra, Hervé Jégou, Julien Mairal, Piotr Bojanowski, and Armand Joulin. Emerging properties in self-supervised vision transformers. In *Proceedings of the International Conference on Computer Vision (ICCV)*, 2021.
- Richard J. Chen, Tong Ding, Ming Y. Lu, Drew F. K. Williamson, Guillaume Jaume, Bowen Chen, Andrew Zhang, Daniel Shao, Andrew H. Song, Muhammad Shaban, Mane Williams, Anurag Vaidya, Sharifa Sahai, Lukas Oldenburg, Luca L. Weishaupt, Judy J. Wang, Walt Williams, Long Phi Le, Georg Gerber, and Faisal Mahmood. A general-purpose self-supervised model for computational pathology, 2023.
- Ting Chen, Simon Kornblith, Mohammad Norouzi, and Geoffrey Hinton. A simple framework for contrastive learning of visual representations. In *Proceedings of the 37th International Conference on Machine Learning, ICML’20*, 2020a.
- X. Chen, S. Xie, and K. He. An empirical study of training self-supervised vision transformers. In *2021 IEEE/CVF International Conference on Computer Vision (ICCV)*, pages 9620–9629, 2021.
- Xinlei Chen, Haoqi Fan, Ross B. Girshick, and Kaiming He. Improved baselines with momentum contrastive learning. *ArXiv*, abs/2003.04297, 2020b.
- Heather Dawson. Digital pathology – rising to the challenge. *Frontiers in Medicine*, page 888896, 2022.
- Jia Deng, Wei Dong, Richard Socher, Li-Jia Li, Kai Li, and Li Fei-Fei. Imagenet: A large-scale hierarchical image database. In *2009 IEEE Conference on Computer Vision and Pattern Recognition*, pages 248–255, 2009.
- Jonas Dippel and Barbara Feulner. Rudolfv: A foundation model by pathologists for pathologists, 0 2024.
- Babak Ehteshami Bejnordi, Mitko Veta, Paul Johannes van Diest, Bram van Ginneken, Nico Karssemeijer, Geert Litjens, Jeroen A. W. M. van der Laak, , and the CAMELYON16 Consortium. Diagnostic Assessment of Deep Learning Algorithms for Detection of Lymph Node Metastases in Women With Breast Cancer. *JAMA*, 318(22):2199–2210, 2017.

- Alexandre Filiot, Ridouane Ghermi, Antoine Olivier, Paul Jacob, Lucas Fidon, Alice Mac Kain, Charlie Saillard, and Jean-Baptiste Schiratti. Scaling self-supervised learning for histopathology with masked image modeling. *medRxiv*, 2023.
- Edna Garcia, Iman Kundu, Melissa Kelly, Ryan Soles, Lotte Mulder, and Geoffrey A. Talmon. The american society for clinical pathology’s job satisfaction, well-being, and burnout survey of pathologists. *American journal of clinical pathology*, pages 435–448, 2020.
- Aritra Ghosh, Himanshu Kumar, and P. Shanti Sastry. Robust loss functions under label noise for deep neural networks. In *AAAI Conference on Artificial Intelligence*, 2017.
- Bo Han, Quanming Yao, Xingrui Yu, Gang Niu, Miao Xu, Weihua Hu, Ivor W. Tsang, and Masashi Sugiyama. Co-teaching: Robust training of deep neural networks with extremely noisy labels. In *Proceedings of the 32nd International Conference on Neural Information Processing Systems, NIPS’18*, page 8536–8546, 2018.
- Kaiming He, X. Zhang, Shaoqing Ren, and Jian Sun. Deep residual learning for image recognition. *2016 IEEE Conference on Computer Vision and Pattern Recognition (CVPR)*, pages 770–778, 2015.
- Kaiming He, Haoqi Fan, Yuxin Wu, Saining Xie, and Ross Girshick. Momentum contrast for unsupervised visual representation learning. In *2020 IEEE/CVF Conference on Computer Vision and Pattern Recognition (CVPR)*, 2020.
- Weiming Hu, Chen Li, Xiaoyan Li, Md Mamunur Rahaman, Jiquan Ma, Yong Zhang, Haoyuan Chen, Wanli Liu, Changhao Sun, Yudong Yao, Hongzan Sun, and Marcin Grzegorzek. Gashissdb: A new gastric histopathology image dataset for computer aided diagnosis of gastric cancer. *Computers in Biology and Medicine*, page 105207, 2022.
- Shengyi Hua, Fang Yan, Tianle Shen, and Xiaofan Zhang. Pathoduet: Foundation models for pathological slide analysis of h&e and ihc stains, 2023.
- Hongyang Jiang, Mengdi Gao, Yan Hu, Qi Ren, Zhaoheng Xie, and Jiang Liu. Label-noise-tolerant medical image classification via self-attention and self-supervised learning. *arXiv preprint arXiv:12306.09718*, 2023.
- Mingu Kang, Heon Song, Seonwook Park, Donggeun Yoo, and Sérgio Pereira. Benchmarking self-supervised learning on diverse pathology datasets. In *Proceedings of the IEEE/CVF Conference on Computer Vision and Pattern Recognition (CVPR)*, pages 3344–3354, 2023.
- Jakob Nikolas Kather, Niels Halama, and Alexander Marx. 100,000 histological images of human colorectal cancer and healthy tissue, May 2018.
- Bidur Khanal, Binod Bhattarai, Bishesh Khanal, and Cristian A. Linte. Improving medical image classification in noisy labels using only self-supervised pretraining. In *DEMI@MICCAI*, 2023.

- Yoo Jung Kim, Hyungjoon Jang, Kyoungbun Lee, Seongkeun Park, Sung-Gyu Min, Choyeon Hong, Jeong Hwan Park, Kanggeun Lee, Jisoo Kim, Wonjae Hong, Hyun Jung, Yanling Liu, Haran Rajkumar, Mahendra Khened, Ganapathy Krishnamurthi, Sen Yang, Xiyue Wang, Chang Hee Han, Jin Tae Kwak, Jianqiang Ma, Zhe Tang, Bahram Marami, Jack Zeineh, Zixu Zhao, Pheng-Ann Heng, Rüdiger Schmitz, Frederic Madesta, Thomas Rösch, Rene Werner, Jie Tian, Elodie Puybareau, Matteo Bovio, Xiufeng Zhang, Yifeng Zhu, Se Young Chun, Won-Ki Jeong, Peom Park, and Jinwook Choi. Paip 2019: Liver cancer segmentation challenge. *Medical Image Analysis*, 67:101854, 2021.
- Alexander Kolesnikov, Alexey Dosovitskiy, Dirk Weissenborn, Georg Heigold, Jakob Uszkoreit, Lucas Beyer, Matthias Minderer, Mostafa Dehghani, Neil Houlsby, Sylvain Gelly, Thomas Unterthiner, and Xiaohua Zhai. An image is worth 16x16 words: Transformers for image recognition at scale. 2021.
- Nikhil Cherian Kurian, S Varsha, Akshay Bajpai, Sunil Patel, and Amit Sethi. Improved histology image classification under label noise via feature aggregating memory banks. In *2022 IEEE 19th International Symposium on Biomedical Imaging (ISBI)*, 2022.
- Kuang-Huei Lee, Xiaodong He, Lei Zhang, and Linjun Yang. Cleannet: Transfer learning for scalable image classifier training with label noise. *2018 IEEE/CVF Conference on Computer Vision and Pattern Recognition*, pages 5447–5456, 2017.
- Junnan Li, Yongkang Wong, Qi Zhao, and M. Kankanhalli. Learning to learn from noisy labeled data. *2019 IEEE/CVF Conference on Computer Vision and Pattern Recognition (CVPR)*, pages 5046–5054, 2018.
- Junnan Li, Richard Socher, and Steven C. H. Hoi. Dividemix: Learning with noisy labels as semi-supervised learning. *ICLR 2020*, 2020.
- Z. Liu, Y. Lin, Y. Cao, H. Hu, Y. Wei, Z. Zhang, S. Lin, and B. Guo. Swin transformer: Hierarchical vision transformer using shifted windows. In *2021 IEEE/CVF International Conference on Computer Vision (ICCV)*, pages 9992–10002, 2021.
- Ilya Loshchilov and Frank Hutter. SGDR: stochastic gradient descent with warm restarts. In *5th International Conference on Learning Representations, ICLR 2017, Toulon, France, April 24-26, 2017, Conference Track Proceedings*, 2017.
- Ming Y. Lu, Bowen Chen, Drew F. K. Williamson, Richard J. Chen, Ivy Liang, Tong Ding, Guillaume Jaume, Igor Odintsov, Andrew Zhang, Long Phi Le, Georg K. Gerber, Anil Parwani, and Faisal Mahmood. Towards a visual-language foundation model for computational pathology. *ArXiv*, abs/2307.12914, 2023.
- Xingjun Ma, Hanxun Huang, Yisen Wang, Simone Romano, Sarah M. Erfani, and James Bailey. Normalized loss functions for deep learning with noisy labels. *ICML2020*, 2020.
- Curtis G. Northcutt, Tailin Wu, and Isaac L. Chuang. Learning with confident examples: Rank pruning for robust classification with noisy labels. In *Proceedings of the Thirty-Third Conference on Uncertainty in Artificial Intelligence, UAI’17*, 2017.

- António Polónia, Catarina Eloy, and Paulo Aguiar. BACH Dataset : Grand Challenge on Breast Cancer Histology images, January 2020.
- Herbert E. Robbins. A stochastic approximation method. *Annals of Mathematical Statistics*, 22:400–407, 1951.
- Cheng Tan, Jun Xia, Lirong Wu, and Stan Z. Li. Co-learning: Learning from noisy labels with self-supervision. *Proceedings of the 29th ACM International Conference on Multimedia*, 2021.
- Bastiaan S Veeling, Jasper Linmans, Jim Winkens, Taco Cohen, and Max Welling. Rotation equivariant CNNs for digital pathology. June 2018.
- Eugene Vorontsov, Alican Bozkurt, Adam Casson, George Shaikovski, Michal Zelechowski, Siqi Liu, Kristen Severson, Eric Zimmermann, James Hall, Neil Tenenholtz, Nicolo Fusi, Philippe Mathieu, Alexander van Eck, Donghun Lee, Julian Viret, Eric Robert, Yi Kan Wang, Jeremy D. Kunz, Matthew C. H. Lee, Jan Bernhard, Ran A. Godrich, Gerard Oakley, Ewan Millar, Matthew Hanna, Juan Retamero, William A. Moyer, Razik Yousfi, Christopher Kanan, David Klimstra, Brandon Rothrock, and Thomas J. Fuchs. Virchow: A Million-Slide Digital Pathology Foundation Model. *arXiv e-prints*, 2023.
- Xiyue Wang, Sen Yang, Jun Zhang, Minghui Wang, Jing Zhang, Junzhou Huang, Wei Yang, and Xiao Han. Transpath: Transformer-based self-supervised learning for histopathological image classification. In *International Conference on Medical Image Computing and Computer-Assisted Intervention*, pages 186–195. Springer, 2021.
- Xiyue Wang, Sen Yang, Jun Zhang, Minghui Wang, Jing Zhang, Wei Yang, Junzhou Huang, and Xiao Han. Transformer-based unsupervised contrastive learning for histopathological image classification. *Medical Image Analysis*, 81:102559, 2022.
- Xiyue Wang, Yuexi Du, Sen Yang, Jun Zhang, Minghui Wang, Jing Zhang, Wei Yang, Junzhou Huang, and Xiao Han. Retccl: Clustering-guided contrastive learning for whole-slide image retrieval. *Medical Image Analysis*, 83:102645, 2023.
- Jerry Wei, Arief Suriawinata, Bing Ren, Xiaoying Liu, Mikhail Lisovsky, Louis Vaickus, Charles Brown, Michael Baker, Naofumi Tomita, Lorenzo Torresani, et al. A petri dish for histopathology image analysis. In *International Conference on Artificial Intelligence in Medicine*, pages 11–24. Springer, 2021.
- John N Weinstein, Eric A Collison, Gordon B. Mills, Kenna M Shaw, Kyle Elrott, Ilya Shmulevich, Chris Sander, and Joshua M Stuart. The cancer genome atlas pan-cancer analysis project. In *Nature genetics*, page 1113–1120, 2013.
- Yihao Xue, Kyle Whitecross, and Baharan Mirzasoleiman. Investigating why contrastive learning benefits robustness against label noise. In *Proceedings of the 39th International Conference on Machine Learning*, volume 162, 2022.
- Xingrui Yu, Bo Han, Jiangchao Yao, Gang Niu, Ivor Wai-Hung Tsang, and Masashi Sugiyama. How does disagreement help generalization against label corruption? In *International Conference on Machine Learning*, 2019.

- Jure Zbontar, Li Jing, Ishan Misra, Yann LeCun, and Stéphane Deny. Barlow twins: Self-supervised learning via redundancy reduction. In *Proceedings of the 38th International Conference on Machine Learning, ICML 2021, 18-24 July 2021, Virtual Event*, Proceedings of Machine Learning Research, 2021.
- Chiyuan Zhang, Samy Bengio, Moritz Hardt, Benjamin Recht, and Oriol Vinyals. Understanding deep learning requires rethinking generalization. *arXiv preprint arXiv:1611.03530*, 2016.
- Zhilu Zhang and Mert R. Sabuncu. Generalized cross entropy loss for training deep neural networks with noisy labels. In *Proceedings of the 32nd International Conference on Neural Information Processing Systems, NIPS’18*, page 8792–8802, 2018.
- Jinghao Zhou, Chen Wei, Huiyu Wang, Wei Shen, Cihang Xie, Alan Yuille, and Tao Kong. ibot: Image bert pre-training with online tokenizer. *International Conference on Learning Representations (ICLR)*, 2022.
- Chuang Zhu, Wenkai Chen, Ting Peng, Ying Wang, and Mulan Jin. Hard sample aware noise robust learning for histopathology image classification. *IEEE transactions on medical imaging*, 2022.

Appendix A. Experimental Settings

As a baseline, we use a ResNet-50 model trained with the CCE loss starting from ImageNet (Deng et al., 2009) weights. For baseline runs we used a stochastic gradient descent (SGD) optimizer (Robbins, 1951) with learning rate of 0.0005 coupled to cosine annealing scheduler (Loshchilov and Hutter, 2017) and early stopping with 20 patience epochs. For GCE, we set q to 0.7 and used the same settings as baseline. For APL, we used the normalized cross entropy - reverse cross entropy (NCE-RCE) loss with $\alpha = 0.6$ and $\beta = 0.4$. For both GCE and APL we did a five epochs warmup with CCE loss. For DivideMix, we used default settings and a learning rate of 0.001 for 50 epochs. For embedding-based trainings, a four-layer linear neural network serves as the classifier model. We used grid search to find out optimal learning rate, batch size, patience and Gaussian noise σ for each backbone-dataset combinations. All runs are conducted on Nvidia GeForce RTX 2080 Ti GPUs.

Appendix B. Datasets Details

NCT-CRC-HE-100K consists of 100,000 hematoxylin and eosin (H&E) stained 224x224 histological images of human colorectal cancer (CRC) divided in 9 tissue classes (adipose,

background, debris, lymphocytes, mucus, smooth muscle, normal colon mucosa, cancer-associated stroma, colorectal adenocarcinoma epithelium). The test set uses a different CRC-VAL-HE-7K dataset consisting of 7,180 patches featuring all nine classes. PatchCamelyon binary dataset contains 327,680 stained 96x96 patches derived from histopathological scans of lymph node sections with positive label indicating presence of metastatic tissue. It provides train, validation and test sets. PatchCamelyon is derived from the Camelyon16 challenge (Ehteshami Bejnordi et al., 2017). BACH dataset is composed of H&E stained breast histology microscopy 2048x1536 patches. Train and test sets respectively possess 400 and 83 patches distributed in 4 classes according to the predominant cancer type in each image (normal, benign, *in situ* carcinoma, invasive carcinoma). As the ground truth was not available for the test set, we asked a breast pathologist expert to label the 100 patches. Among the 100, 17 were considered uncertain due to a lack of contextual information on the patch so we chose to not use these 17 patches in order to have a clean ground truth. MHIST is made up of 3,152 H&E stained 224x224 images of colorectal polyps split into 2175 and 977 for train/test sets. Binary classes, hyperplastic polyp (HP) or sessile serrated adenoma (SSA), indicate the predominant histological pattern. LC25000 dataset contains five classes of 5,000 768x768 images of lung and colon tissues. The classes are: colon adenocarcinomas, benign colonic tissues, lung adenocarcinomas, lung squamous cell carcinomas and benign lung tissues. GasHisSDB consists of 32,284 160x160 H&E stained gastric cancer pathology patches. Classes are abnormal and normal. In these two last datasets there is no test set provided so we split ourselves train set into 80:20 for train/test sets then 80:20 for train/validation sets.

For image training methods, we employ a traditional preprocessing and augmentation pipeline. For the training set, we incorporate resizing, horizontal and vertical flipping, color jittering, and normalization. For the validation and test sets, we simplify the process by only resizing and normalizing the images. The resizing dimensions are set to 512x512 for BACH and LC25000 datasets, while for the remaining datasets, we maintain the original sizes.

For embedding extractions, we consider the fact that backbones require an input size of 224x224. Therefore, for oversized images, such as those in the BACH and LC25000 datasets, we resize them to this resolution. For undersized images, like those in the PatchCamelyon and GasHisSDB datasets, we experiment with both resizing and padding. Our results indicate that resizing yields better outcomes. The size of the embeddings varies depending on the backbone used. For Phikon, CTransPath, and PathoDuet, the embedding size is 768, while for RetCCL and Lunit-BT, it is 2048. Lunit-DINO, on the other hand, uses an embedding size of 384.

For training methods based on embeddings, we introduce an additional augmentation to the training set by adding random Gaussian noise, scaled with σ .

Appendix C. Asymetric Noise Transition Matrices

Table 4: NCT-CRC-HE-100k class transition matrix.

	ADI	BACK	DEB	LYM	MUC	MUS	NORM	STR	TUM
ADI	$1 - \eta$	0	0	0	0	$\frac{\eta}{2}$	$\frac{\eta}{2}$	0	0
BACK	0	$1 - \eta$	$\frac{\eta}{3}$	$\frac{\eta}{3}$	$\frac{\eta}{3}$	0	0	0	0
DEB	0	$\frac{\eta}{3}$	$1 - \eta$	$\frac{\eta}{3}$	$\frac{\eta}{3}$	0	0	0	0
LYM	0	$\frac{\eta}{3}$	$\frac{\eta}{3}$	$1 - \eta$	$\frac{\eta}{3}$	0	0	0	0
MUC	0	$\frac{\eta}{3}$	$\frac{\eta}{3}$	$\frac{\eta}{3}$	$1 - \eta$	0	0	0	0
MUS	$\frac{\eta}{2}$	0	0	0	0	$1 - \eta$	$\frac{\eta}{2}$	0	0
NORM	$\frac{\eta}{2}$	0	0	0	0	$\frac{\eta}{2}$	$1 - \eta$	0	0
STR	0	0	0	0	0	0	0	$1 - \eta$	η
TUM	0	0	0	0	0	0	0	η	$1 - \eta$

Table 5: BACH class transition matrix.

	Benign	CIS	CI	Normal
Benign	$1 - \eta$	η	0	0
CIS	$\frac{\eta}{2}$	$1 - \eta$	$\frac{\eta}{2}$	0
CI	0	$\frac{\eta}{2}$	$1 - \eta$	$\frac{\eta}{2}$
Normal	0	0	η	$1 - \eta$

Table 6: LC25000 class transition matrix.

	Colon ACA	Benign Colon	Lung ACA	Benign Lung	Lung SCC
Colon ACA	$1 - \eta$	$\frac{\eta}{2}$	$\frac{\eta}{2}$	0	0
Benign Colon	$\frac{\eta}{2}$	$1 - \eta$	0	$\frac{\eta}{2}$	0
Lung ACA	$\frac{\eta}{2}$	0	$1 - \eta$	0	$\frac{\eta}{2}$
Benign Lung	0	η	0	$1 - \eta$	0
Lung SCC	0	0	η	0	$1 - \eta$